Urolithiasis (2024) 52:164
https://doi.org/10.1007/s00240-024-01655-3

RESEARCH

Comprehensive analysis and validation of TP73 as a biomarker for calcium oxalate nephrolithiasis using machine learning and in vivo and in vitro experiments

Zijian Zhou[1,2] · Lujia Wang[1,2] · Lingkai Cai[3] · Peng Gao[1,2] · Hongcheng Lu[4] · Zhong Wu[1,2]

Received: 14 August 2024 / Accepted: 26 October 2024

Abstract

Calcium oxalate (CaOx) nephrolithiasis constitutes approximately 75% of nephrolithiasis cases, resulting from the supersaturation and deposition of CaOx crystals in renal tissues. Despite their prevalence, precise biomarkers for CaOx nephrolithiasis are lacking. With advances in high-throughput sequencing, we aimed to identify biomarkers of CaOx nephrolithiasis by combining two CaOx nephrolithiasis datasets (GSE73680 and GSE117518). Utilizing weighted gene co-expression network analysis (WGCNA) and four machine learning, we identified six hub genes (DLK2, BHLHA15, C12orf5, ICMT, LOXHD1, and TP73) as potential biomarkers. Additionally, CIBERSORT immune infiltration analysis suggested that these core genes may influence immune cell recruitment and infiltration in CaOx nephrolithiasis. Then, TP73 emerged as a significant hub gene in CaOx nephrolithiasis via receiver operating characteristic (ROC) analysis (AUC = 0.885). Furthermore, the role of TP73 was validated in CaOx nephrolithiasis rat models induced by 1% ethylene glycol, as well as clinical samples and renal tubular epithelial cell models treated with 1 mM oxalate. Immunohistochemistry, RNA-Sequencing, and RT-qPCR experiments demonstrated an increased expression of TP73 in CaOx nephrolithiasis rat models and clinical samples. After transfection with TP73 lentivirus, CCK-8 assays suggested that TP73 could inhibit the proliferation of HK-2 and NRK-52E cells. In oxalate-induced cell models, dihydroethidium staining and flow cytometry apoptosis assays indicated that TP73 could enhance ROS levels and cell apoptosis. In summary, our study preliminarily identified TP73 as a diagnostic biomarker and elucidated the promoting role of TP73 in CaOx nephrolithiasis, providing a deeper understanding of the clinical diagnosis and pathogenesis.

Keywords Calcium oxalate nephrolithiasis · Machine learning · TP73 · Biomarker · Oxalate-induced cell model · RNA-Sequencing

Introduction

Nephrolithiasis, a prevalent global disorder, induces severe pain, substantially diminishing patients' quality of life [1]. Furthermore, the global incidence of this disease

Zijian Zhou, Lujia Wang, and Lingkai Cai contributed equally to this work.

✉ Hongcheng Lu
lhc@njmu.edu.cn

✉ Zhong Wu
drzhongwu2020@163.com

[1] Department of Urology, Huashan Hospital, Fudan University, 12 Middle Wulumuqi Rd, Shanghai 200040, People's Republic of China

[2] Clinical Research Center of Urolithiasis, Shanghai Medical College, Fudan University, Shanghai 200040, People's Republic of China

[3] Department of Urology, The First Affiliated Hospital of Nanjing Medical University, Nanjing 210000, People's Republic of China

[4] Department of Urology, The Affiliated Wuxi People′s Hospital of Nanjing Medical University, Wuxi People′s Hospital, Wuxi Medical Center, Nanjing Medical University, Wuxi 214023, People's Republic of China

Published online: 16 November 2024

is escalating, with a recurrence rate exceeding 45% [2]. Approximately 75% of nephrolithiasis is primarily comprised of calcium oxalate (CaOx), and CaOx nephrolithiasis represents a prevalent disorder within urology, with multifaceted etiology encompassing factors such as urethral anatomy, sex, diet, geographical location, and seasonal influences [3]. Contemporary hypotheses suggest that the supersaturation and deposition of CaOx crystals in renal tissues contribute to the apoptosis and injury of kidney tubular cells, thereby promoting the continued formation of CaOx nephrolithiasis [4].

Cell apoptosis, also known as programmed cell death, is a process by which cells undergo a controlled and regulated self-destruction mechanism [5]. Previous studies have reported that cell apoptosis is crucial in CaOx kidney stone formation process where cellular injury can expose matrix components or release debris that facilitates crystal nucleation, while cell apoptosis can modify the local chemical environment, thereby promoting crystallization [6, 7]. Moreover, in recent years, high-throughput sequencing and machine learning have emerged as pivotal tools for identifying biomarkers, shedding light on the molecular mechanisms underlying disease progression [8–12], including kidney stone disease [13–15]. Hence, using sequencing methods with machine learning could identify diagnostic markers for CaOx nephrolithiasis.

In this study, the only two existing gene expression omnibus (GEO) datasets of CaOx nephrolithiasis patients were combined, including GSE73680 and GSE117518. To screen the hub genes in CaOx kidney stones, weighted gene co-expression network analysis (WGCNA) and four machine-learning were used: random forests (RF), least absolute shrinkage and selection operator (Lasso), support vector machine-recursive feature elimination (SVM-RFE), and Boruta. Of these, TP73 was proved most significant and was thus chosen for further characterization and experimental validation. Currently, the role of the TP73 gene in CaOx nephrolithiasis remains elusive. Hence, this study aims to confirm the regulatory influence of TP73 in this process, offering a new biomarker of CaOx kidney stones.

Materials and methods

Gene expression profiles and data analysis

Accessing the GEO database, two different datasets of CaOx stone patients were employed (Table 1), including GSE73680 (Gene expression profile of Randall's Plaque tissue) [16] and GSE117518 (Cui Y, Zu X, Chen H. 2018. Microarray analysis of long noncoding RNA and mRNA expression profiles in Randall's Plaques of CaOx stones patients. Gene Expression Omnibus. https://www.ncbi.nlm.nih.gov/geo/query/acc.cgi?acc=GSE117518). The GSE73680 dataset consists of 6 normal renal papillary tissues from individuals without a history of kidney stones (referred to as the Normal group) and 24 Randall's Plaques (RPs) from patients with calcium stones (referred to as the CaOx group). Human renal papillary tip tissues were biopsied during endoscopic kidney stone surgery. The GSE117518 dataset consists of 3 normal renal papillary tissues from individuals without a history of kidney stones (also referred to as the Normal group) and 3 RPs from patients with calcium stones (also referred to as the CaOx group). Normal renal papillary tissues were obtained from patients with renal tumor who underwent nephrectomy, the tissues were obtained from papillary without tumor invasion. RPs of CaOx renal stones patients were obtained from patients with idiopathic CaOx renal stone who underwent percutaneous nephrolithotomy. To combine GSE73680 and GSE117518, we normalized the data and then corrected the expression values for batch effects using the sva R package [17]. The schematic flowchart of this study was shown in Fig. 1. A volcano plot was produced to highlight the differentially expressed genes (DEGs) between the CaOx group and the Normal group based on the criteria of $|Log^2$ Fold-Change$| \geq 0.582$ and P value < 0.05.

Weighted gene co-expression network analysis (WGCNA)

We began by computing pairwise correlations between all genes in the dataset to establish the foundation for constructing the co-expression network. Then, using the formula

Table 1 The datasets used in this article

GEO series	Platform	Normal group ($n=9$)	CaOx group ($n=27$)
GSE73680	GPL17077	Normal papillary tissues from control patients without any kidney stone ($n=6$)	Randall's Plaque from calcium stone former ($n=24$)
GSE117518	GPL21827	Normal papillary tissues from patients with renal tumor without invasion ($n=3$)	Randall's Plaque tissues of CaOx renal stones patients ($n=3$)

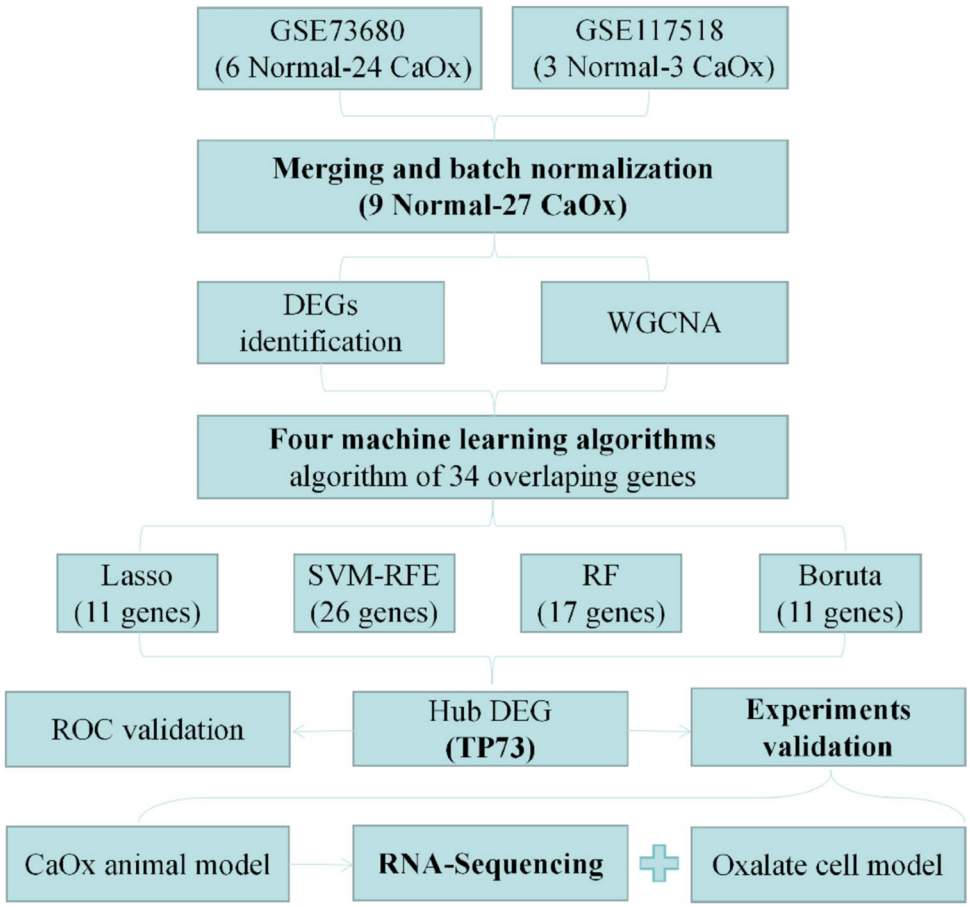

Fig. 1 The schematic flowchart of this study

amn = |cmn|β, where cmn represents Pearson's correlation between gene m and gene n, we constructed a weighted adjacency matrix. Next, we calculated different β values to assess the scale-free topology fit index and select the one that best achieved a scale-free network. To evaluate the scale-free topology fit index and select the optimal β value, we computed various β values. Subsequently, we calculated the topological overlap measure (TOM) matrix, which quantifies a gene's network connectivity by summing its adjacency values with all other genes. Genes exhibiting similar expression profiles were clustered into gene modules using average linkage hierarchical clustering. For each gene, we determined gene significance (GS) and module membership (MM) in relation to clinical traits. GS represents the correlation between gene expression and the clinical trait, whereas MM indicates the degree of connectivity of a gene within its module. The modules associated with CaOx nephrolithiasis were identified by evaluating the coefficient of determination ($R^2 > 0.9$) and statistical significance ($P < 0.05$).

Machine learning

To further screen the hub DEGs, four machine learning algorithms were employed: random forests (RF), least absolute shrinkage and selection operator (Lasso), support vector machine-recursive feature elimination (SVM-RFE), Boruta [18]. The RF algorithm was implemented using the randomForest R package, while Lasso regression was performed with tenfold cross-validation using the glmnet R package [19]. Feature selection was conducted using the Boruta algorithm with the Boruta R package, while the caret R package was used for SVM-RFE [20]. Lastly, the six hub DEGs (DLK2, BHLHA15, C12orf5, ICMT, LOXHD1, and TP73) were selected among multiple machine learnings with Venn plot. The predictive capability of the algorithms was assessed using receiver operating characteristic (ROC) curves, with the area under the curve (AUC) calculated to quantify their performance. The performance of the predictive models was evaluated in terms of discrimination, calibration, and clinical utility. Calibration was visually assessed using graphical representations of the consistency, and clinical utility was investigated through decision curve analysis (DCA).

Evaluation and correlation analysis of infiltration-related immune cells

Using the CIBERSORT algorithm, 22 types of immune cell matrices were filtered. The Spearman correlation between the hub genes and infiltrating immune cells was analyzed. The results were illustrated using the ggstatsplot and ggplot2 R packages.

CaOx nephrolithiasis rat models and histologic analysis

Male Sprague–Dawley (SD) rats aged 5–6 weeks were given a one-week acclimation period before the start of the experiment. The study was approved by the Fudan Laboratory Animal Ethics Board. Initially, 10 SD rats were divided equally into two groups: the control group (named Con, n = 5), and the CaOx group (named CaOx, n = 5). The control group had access to water ad libitum, while the CaOx group received 1% ethylene glycol (EG) in their drinking water. After four weeks, the renal tissues, serum and urine were collected for further analysis. Hematoxylin & eosin (HE) staining was used to observe renal morphology and injury, while Alizarin Red (AR) staining in pH = 6.8 was used to detect calcium deposits as previously described [21]. Urinary levels of Ca^{2+} and Mg^{2+}, and renal function (serum creatinine: Scr, blood urea nitrogen: BUN) were analyzed using an automatic biochemical analyzer (Servicebio, Wuhan, China).

RNA-Sequencing (RNA-Seq) and enrichment analysis

TRIzol reagent was used to extract total RNA from the kidneys of rats (n = 3 per group). The purity and quantity of RNA were assessed with a Nanodrop spectrophotometer and SDS gel electrophoresis. The cDNA samples were randomly fragmented, and the libraries were loaded onto a flow cell for cluster generation. Sequencing was performed on an Illumina HiSeq 4000. RNA-Seq analysis was conducted by Biofifile (Shanghai, China). The DEGs were selected based on the cut-off criteria of $P < 0.05$ and | fold-change |> 1.5. Moreover, GO and KEGG pathway analysis were conducted for the DEGs with the clusterProfiler and enrichplot R packages with an adjust P value < 0.05. Gene Set Enrichment Analysis (GSEA) of the KEGG pathway was carried out using the clusterProfiler R package, considering in terms of normalized enrichment scores (NES) with an adjust P value < 0.05 and false discovery rate (FDR) < 0.25.

Clinical samples

Tissue samples were collected at Huashan Hospital, Fudan University, Shanghai, China. For the CaOx kidney stone group (CaOx, n = 3), RPs were derived from patients with CaOx kidney stones undergoing ureteroscopy. Correspondingly, renal papillary tissues for the normal control group (NC, n = 3) were procured from adjacent non-neoplastic kidney tissue of patients undergoing radical nephrectomy without tumor invasion. The study received approval from the Huashan Institutional Review Board of Fudan University (HIRB), and all participants provided informed consent. Immunohistochemistry (IHC) assay was applied to detect TP73 and androgen receptor (AR) expression levels in the renal tissues with rabbit monoclonal anti-TP73 antibody (Abcam, ab189896) and anti-AR antibody (Proteintech, 22,089-1-AP). Dual immunofluorescence staining of TP73 and AR in renal papillary tissues from clinical samples was done to highlight the structural information of TP73 toward RPs development.

Cell culture and lentiviral transduction

The HK-2 and NRK-52E cell lines were obtained from the Chinese Academy of Sciences and cultured in DMEM/F12 and DMEM medium, respectively. For lentiviral transduction, HK-2 and NRK-52E cells were plated in 6-well dishes at 40% confluence and then infected with either a TP73 overexpression lentivirus (termed TP73) or a negative control lentivirus (termed NC). The efficiency of each transfection was assessed using RT-qPCR and western blot assays. The renal tubular epithelial cells were treated with 1 mmol/L oxalate for 24 h as previously published.

Real-time quantitative PCR (RT-qPCR), and western blot assays

The RT-qPCR was performed using the SYBR Green PCR system (Vazyme, Nanjing, China). The sequences of TP73 primers were list in Table S1. Proteins from whole cell lysates were separated on a 10% SDS-PAGE gel and transferred onto a polyvinylidene difluoride (PVDF) membrane. After incubated with 5% skim milk in Tris-buffered saline with Tween 20 (TBST) at room temperature for 2 h, the membrane was incubated overnight at 4 °C with a rabbit monoclonal anti-TP73 antibody (Abcam, ab189896, 1:5000). After incubation with a secondary antibody and subsequent washes with TBST, protein bands were visualized using a gel imaging system.

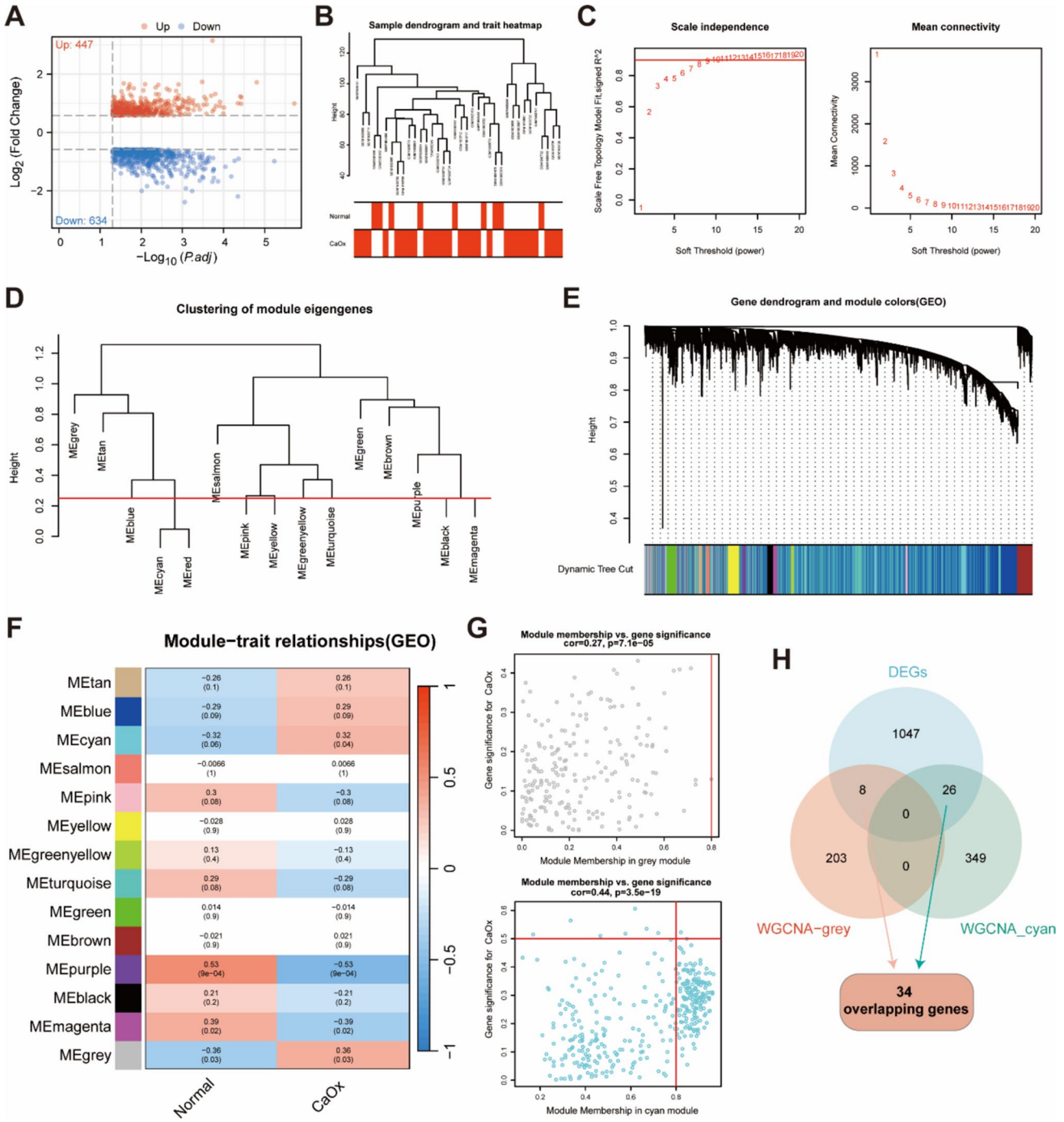

Fig. 2 Identification of differentially expressed genes (DEGs) and screening of hub DEGs via WGCNA based on GEO datasets. **A** Volcano plot displaying all DEGs between the Normal and CaOx groups. **B** Hierarchical clustering tree illustrating gene expression patterns between the Normal and CaOx groups. **C** Determination of the power value: the red line represents $R^2 > 0.9$ when the power value β is 9. **D** Module eigengene dendrogram depicting relationships among modules identified through clustering analysis. **E** Clustering dendrogram and merging of the gene co-expression modules. **F** Heatmap showing correlations between modules and clinical traits, with correlation coefficients and *P* values displayed at the intersections. **G** Significant correlation between module membership (MM) and gene significance (GS) of the cyan and grey modules in the CaOx group. **H** Venn diagram illustrating the intersection between DEGs and genes in modules associated with CaOx nephrolithiasis

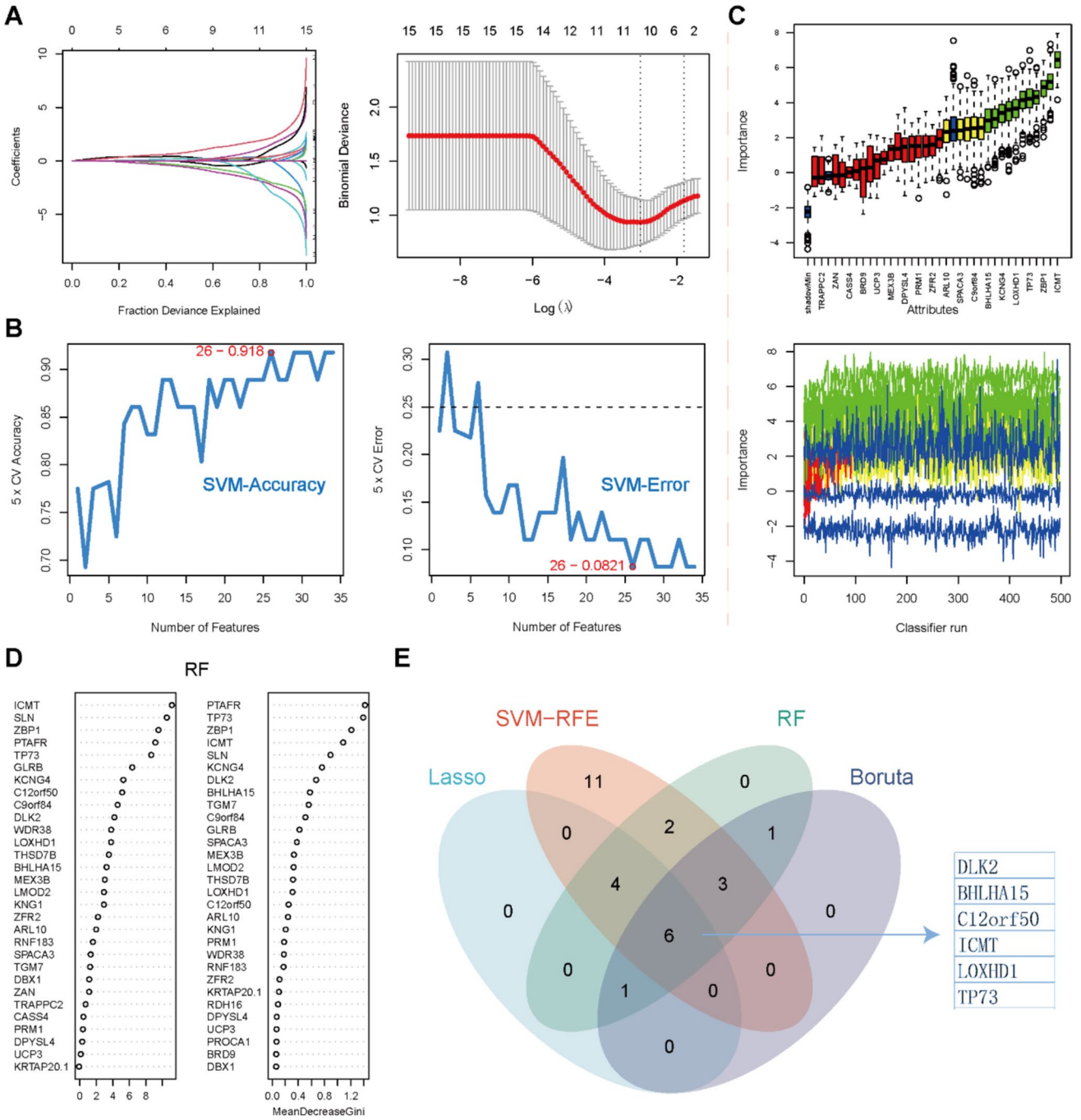

Fig. 3 Screening of hub DEGs via machine learning. **A** Lasso regression of the 34 overlapping DEGs. Vertical dashed lines are plotted at the best lambda. **B** SVM-RFE algorithm obtained 26 DEGs as potential diagnostic biomarkers. **C** The Boruta method plots displayed the DEGs associated with CaOx nephrolithiasis. **D** Top 30 DEGs ranking of the relative importance of genes in the RF classifier. **E** The Venn plot showed the intersected 6 hub DEGs (DLK2, BHLHA15, C12orf5, ICMT, LOXHD1, and TP73) among four machine learning algorithms

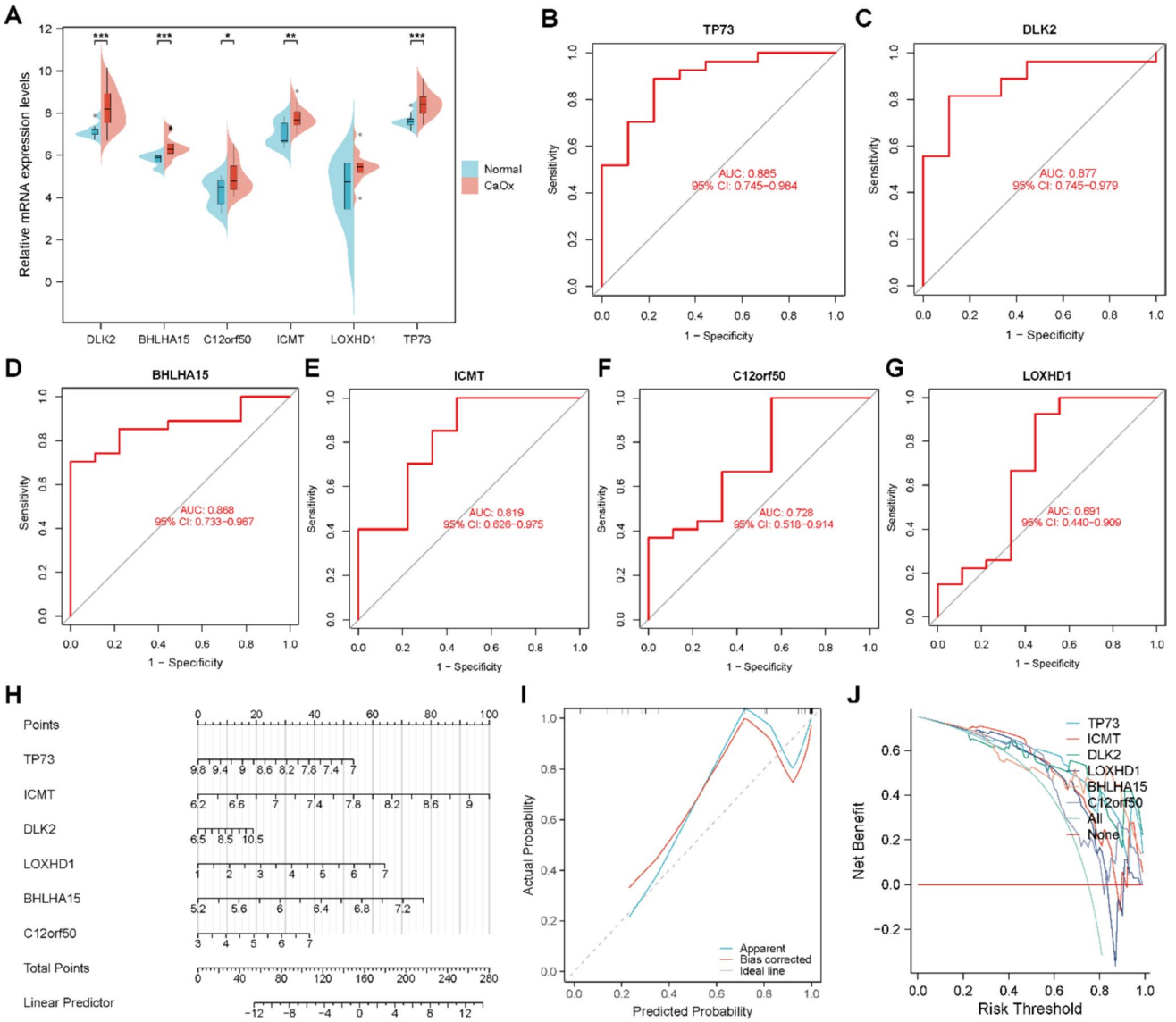

Fig. 4 Hub genes for CaOx nephrolithiasis diagnosis. **A** Bean plot displaying the differential expression of hub DEGs between the Normal and CaOx groups. **B**–**G** ROC curves of hub DEGs for diagnosing CaOx nephrolithiasis. **H** Nomogram used for predicting the occurrence of CaOx nephrolithiasis. **I** Calibration curve for verifying the efficacy of the nomogram. **J** DCA curve for verifying the diagnostic efficacy

Cell Counting Kit-8 (CCK-8), Dihydroethidium (DHE) staining, and flow cytometry apoptosis assays

The initial HK-2 or NRK-52E cells were seeded at equal densities (2×10^3 cells) into 96-well plates following cell counting using trypan blue exclusion. After different treatment, 10 µl of CCK-8 solution was added at specified time points, and cell proliferation was assessed after 24, 48, 72, and 96 h by measuring absorbance at 450 nm using a Multiskan G0 microplate reader (Thermo Fisher Scientific, Finland).

Dihydroethidium (DHE) staining followed by microfluorimetry detection was employed to quantify reactive oxygen species (ROS) production. The treated cells were exposed to 10 µM DHE for 60 min at 37 °C. Subsequently, fluorescence emission was observed after sealing with an anti-fluorescence quencher. ROS production was visualized using an inverted fluorescence microscope (TECAN, Switzerland).

Flow cytometry analysis was conducted to evaluate cell apoptosis using an Annexin V-Fluorescein Isothiocyanate (FITC) Apoptosis Detection kit. Following 24 h of oxalate treatment, HK-2 and NRK-52E cells were trypsinized, washed twice with PBS, and resuspended in 500 µl of binding buffer. Annexin V-FITC and propidium iodide (PI) were added to the cell suspension, mixed gently, and the cells were incubated for 30 min at room temperature in the dark.

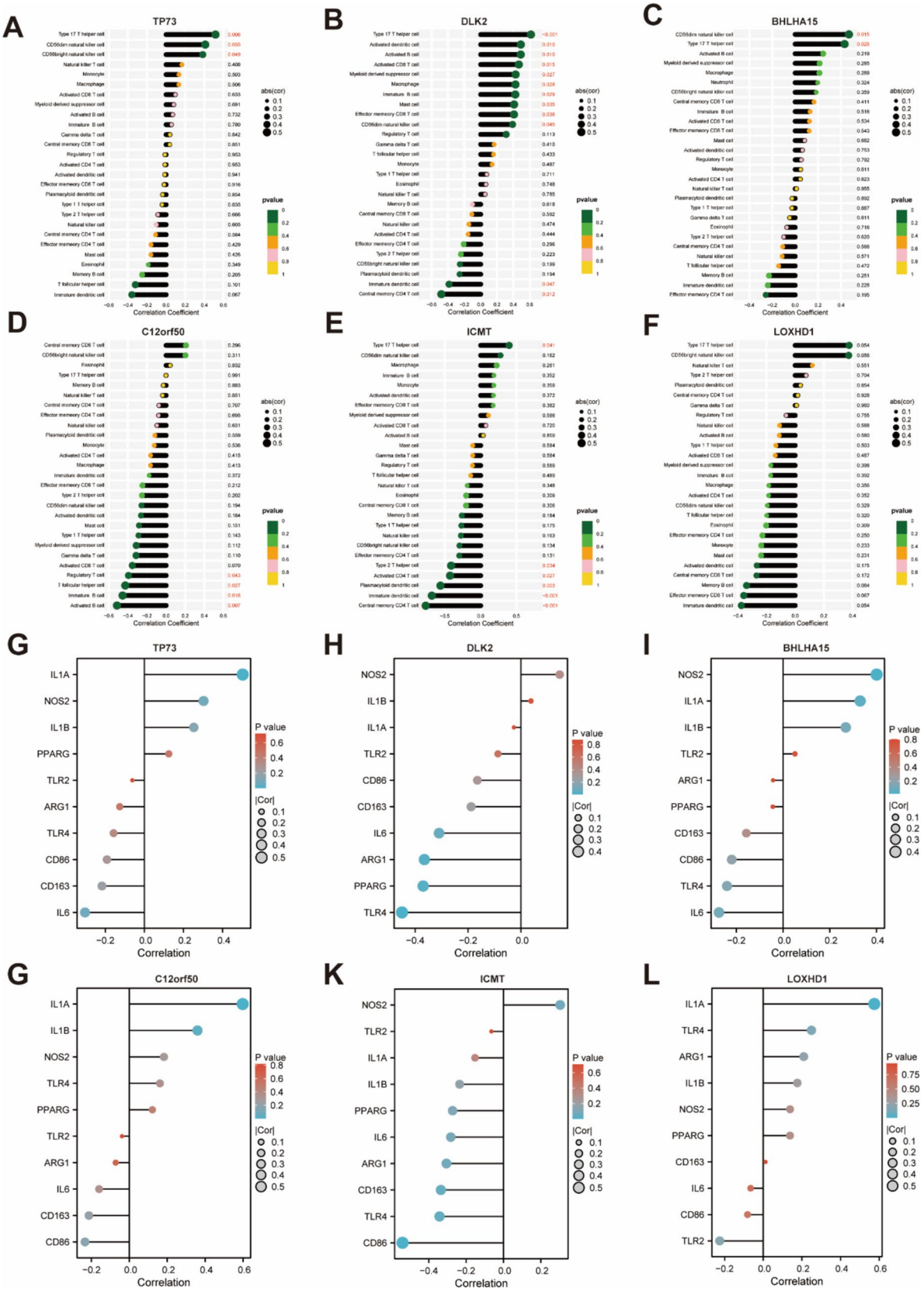

Fig. 5 Correlation between hub genes and immune cells. **A**–**B** Lollipop plot of the correlation between hub genes and immune cells (**A**) and inflammatory markers (**B**)

Table 2 Biochemical Analysis of the levels of SCr, BUN, urine Ca^{2+} and Mg^{2+} in rats

Characteristics	Con group ($n=5$)	CaOx group ($n=5$)	P value
BUN (mg/dL)	21.648 ± 3.847	43.925 ± 14.170	0.010*
Scr (μmol/L)	20.660 ± 5.195	53.023 ± 20.410	0.009**
Urine Ca^{2+} (mmol/l)	1.712 ± 0.153	2.160 ± 0.191	0.003**
Urine Mg^{2+} (mmol/l)	2.288 ± 0.301	1.440 ± 0.613	0.024*

*$P<0.05$, **$P<0.01$, *BUN* Blood urea nitrogen, *Scr* Serum creatinine, *Ca^{2+}* Calcium, *Mg^{2+}* Magnesium

Apoptosis was then analyzed by flow cytometry using a Becton Dickinson system.

Statistical analysis

Statistical analysis was performed using R software (version 4.1.3) and GraphPad Prism (version 9.5). The Wilcoxon test, and Student's t-test, were used to compare two independent groups, respectively.

Results

Identification of DEGs and screening of hub DEGs via WGCNA

The flowchart was presented in Fig. 1. The detailed information of GSE73680 and GSE117518 is displayed in Table 1. After combining GSE73680 and GSE117518, we included 9 samples in the Normal group and 27 samples in the CaOx group. With the threshold of |Log2 FoldChange| ≥ 0.582 and $P<0.05$, there are 1081 DEGs between the Normal group and the CaOx group (Table S2), and 447 of them were significantly upregulated in the CaOx group, while 634 of them were significantly downregulated (Fig. 2A). GO and KEGG analysis showed that these DEGs were mainly involved in external encapsulating structure organization, extracellular matrix organization, extracellular structure organization, and so on (Fig. S1A). GSEA analysis showed that these DEGs were mainly involved in Focal adhesion, ECM − receptor interaction, and else (Fig. S1B). Detailed information of enrichment pathways was listed in Table S3-4.

Then, we utilized WGCNA to identify modules associated with CaOx nephrolithiasis. Figure 2B displayed the hierarchical clustering tree of gene expression patterns between Normal and CaOx groups. A soft threshold power value $\beta=9$ was set to construct a scale-free network (Fig. 2C). Subsequently, the module eigengene dendrogram illustrated the relationships among modules identified through clustering analysis (Fig. 2D). Genes were grouped into 14 modules using hierarchical clustering analysis and dynamic branch cut methods for gene dendrograms (Fig. 2E-F). Among the 14 modules, the grey module ($r=0.27$, $P<0.05$) and the cyan module ($r=0.44$, $P<0.05$) demonstrated a significantly positive correlation with CaOx nephrolithiasis (Fig. 2G). Among them, we identified 211 genes of grey module (Table S5) and 375 genes of cyan module (Table S6) within the CaOx nephrolithiasis-related modules. Finally, 34 overlapping genes were picked with the Venn plot taking the intersection of WGCAN and DEGs (Fig. 2H).

Screening of the hub DEGs via machine learning

We further conducted Lasso regression analysis to identify 11 potential hub DEGs associated with CaOx nephrolithiasis using the expression profiles of 34 DEGs (Fig. 3A). As shown in Fig. 3B, 26 DEGs obtained as potential diagnostic biomarkers by SVM-RFE algorithm. The Boruta method plots showed three blue box-plot for the minimum, mean and maximum attributes (Fig. 3C). The green boxplots represent confirmed important attributes, while the red boxplots indicate attributes confirmed to be unimportant. Yellow boxplots are considered tentative, as the algorithm did not reach a conclusive determination regarding their importance. Additionally, the importance history graph shows that the green boxplots exhibit significantly higher importance compared to the blue shadow. Finally, the Boruta algorithm identified 11 potential hub DEGs associated with CaOx nephrolithiasis. RF identified the top 30 DEGs were in descending order of their relative relevance (Fig. 3D). The specific genes picked from each algorithm were listed in Table S7. Last, the intersected six hub DEGs (DLK2, BHLHA15, C12orf5, ICMT, LOXHD1, and TP73) were picked with Venn plot via the four machine learnings (Fig. 3E).

Hub genes for CaOx nephrolithiasis diagnosis

Except LOXHD1, we observed a significant increased expression of DLK2, BHLHA15, C12orf5, ICMT, and TP73 in the CaOx group (Fig. 4A). To evaluate the diagnostic performance of these hub DEGs, ROC curves were constructed, revealing that TP73 achieved the highest AUC value of 0.885 (Fig. 4B-G), indicating its potential diagnostic value for CaOx nephrolithiasis. Subsequently, nomogram models

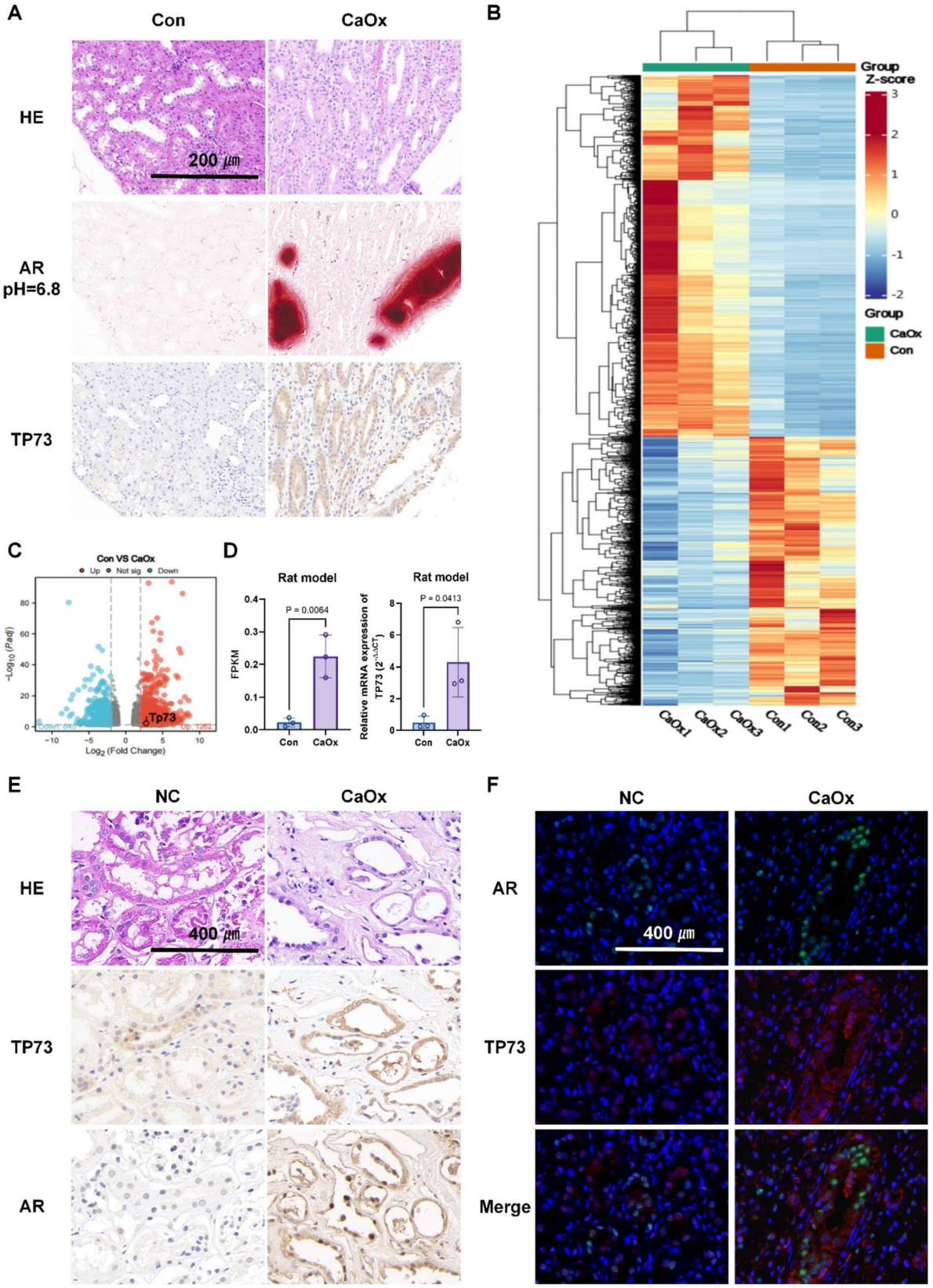
A
Con
CaOx
HE
AR
pH=6.8
TP73
200 μm
B
Group
Z-score
3
2
1
0
-1
-2
Group
CaOx
Con
CaOx1
CaOx2
CaOx3
Con1
Con2
Con3
C
Con VS CaOx
Up
Not sig
Down
Tp73
-Log10 (Padj)
Log2 (Fold Change)
D
Rat model
P = 0.0064
FPKM
Con
CaOx
Rat model
P = 0.0413
Relative mRNA expression of TP73 (2^-ΔΔCT)
Con
CaOx
E
NC
CaOx
HE
TP73
AR
400 μm
F
NC
CaOx
AR
TP73
Merge
400 μm

◂**Fig. 6** Validation of TP73 in CaOx nephrolithiasis rat models and clinical samples. **A** Pathological sections, including HE and AR staining, reveal kidney injury and crystal deposition extent; IHC staining demonstrates TP73 protein expression in Con and CaOx groups (magnification × 20; scale bar, 200 μm). **B–C** Heatmap (**B**) and volcano plot (**C**) analysis of DEGs between Con and CaOx groups using RNA-Seq of rat renal tissues. **D** TP73 mRNA expression in Con and CaOx groups by RNA-Seq and RT-qPCR. **D** TP73 mRNA expression in Con and CaOx groups by RNA-Seq and RT-qPCR. **E** HE and IHC assays of renal papillary tissues from clinical samples (magnification × 40; scale bar, 400 μm). **F** Dual immunofluorescence staining of AR and TP73 of renal papillary tissues from clinical samples (magnification × 40; scale bar, 400 μm)

were developed based on these six hub genes for diagnosing the condition (Fig. 4H). The calibration curve (Fig. 4I) and DCA curve (Fig. 4J) demonstrated that the nomogram model provided superior clinical benefits.

Infiltration of immune cells results

Using the CIBERSORT algorithm, Spearman correlation analysis revealed that TP73, DLK2, BHLHA15, C12orf5, and ICMT had a significant association with a diverse range of immune cells (Fig. 5). TP73 exhibited a significantly positive correlation with Th17 helper cells and CD 56NK cells (Fig. 5A). Except LOXHD1 and C12orf5, DLK2, BHLHA15, and ICMT were all positively correlated with Th17 helper cells as well, ($P < 0.05$, Fig. 5A). Regarding inflammatory markers, TP73, BHLHA15, C12orf5, and LOXHD1 were positively correlated with IL-1A, while ICMT and DLK2 were positively correlated with NOS2 (Fig. 5B).

Validation of TP73 in CaOx nephrolithiasis rat models and clinical samples

Since TP73 obtained the highest AUC values, we picked TP73 as the biomarker of CaOx nephrolithiasis. To investigate the expression of TP73 in CaOx nephrolithiasis, the EG-induced CaOx nephrolithiasis rat models were constructed. The levels of Scr and BUN in the CaOx group were significantly elevated compared to the control group. Specifically, the serum levels of BUN increased from 21.648 ± 3.847 mg/dL in the Con group to 43.925 ± 14.170 mg/dL in the CaOx group. Similarly, the Scr levels rose from 20.660 ± 5.195 μmol/L in the Con group to 53.023 ± 20.410 μmol/L in the CaOx group (Table 2). In the urine, the calcium ion levels increased while the magnesium ion levels decreased in the CaOx group. Moreover, in CaOx rats' kidney tissues, HE and AR staining demonstrated the presence of tubular dilation and injury, and the presence of CaOx crystals in the renal tubules of the CaOx rats (Fig. 6A), and these findings confirm the successful establishment of the CaOx nephrolithiasis rat models.

Furthermore, IHC results displayed an increased TP73 expression in the CaOx group (Fig. 6A). Then, based on the RNA-Seq of rats' kidneys, the heatmap of DEGs between the Con and CaOx group was shown in Fig. 6B. Compared with the Con group, 2362 genes (including TP73) were significantly up-regulated and 1749 genes were down-regulated in the CaOx group (Fig. 6C). Consistently, RNA-Seq and RTq-PCR results displayed an increased TP73 expression in the CaOx group (Fig. 6D). The detailed information of these DEGs was list in Table S8. GO and KEGG analysis showed that these DEGs were mainly involved in immune response, cell adhesion molecules, and so on (Fig. S2A-B). Similarly, GSEA analysis showed that these DEGs were mainly involved in TNF signaling pathway, cell adhesion molecules, and else (Fig. S3).

In clinical samples, HE and IHC analysis were performed to examine the protein expression of TP73 and AR in patients with CaOx stones compared to non-stone patients, and the results revealed an increased protein expression of TP73 in the RPs of CaOx stone patients (Fig. 6E). Meanwhile, we conducted the dual immunofluorescence staining of AR and TP73 of renal papillary tissues from clinical samples, providing clearer evidence of TP73 and AR expression and location near RPs (Fig. 6F). Consistent with bioinformatics screening results, these findings strongly suggest that TP73 is a potential biomarker in CaOx nephrolithiasis.

Function of TP73 in oxalate-induced cell models

After different lentivirus transfection, the expression of TP73 was measured by RT-qPCR and western blot assays in HK-2 (Fig. 7A) or NRK-52E (Fig. 7B) cells. RT-qPCR and western blot analyses demonstrated a marked elevation of TP73 after TP73 lentivirus transfection (Fig. 7A-B). The CCK-8 assay revealed that TP73 could inhibit the proliferation of both HK-2 and NRK-52E cells (Fig. 7C), especially after the oxalate treatment (Fig. 7D). Subsequently, the DHE staining showed that TP73 could enhance the generation of ROS after oxalate treatment (Fig. 7E). The flow cytometry assays demonstrated that TP73 significantly increased the apoptosis of oxalate-induced cells (Fig. 7F). These data suggested the cytotoxic effect of TP73 in oxalate-induced renal tubular epithelial cells, indicating its promoting role in CaOx stone formation.

Discussion

The high recurrence rates and complications significantly increase the physical and psychological burdens on CaOx nephrolithiasis patients [22]. Therefore, it is urgent to find biomarkers and understanding the pathogenesis of CaOx nephrolithiasis is crucial. In this investigation, we delved into the role of the hub gene TP73 in CaOx nephrolithiasis

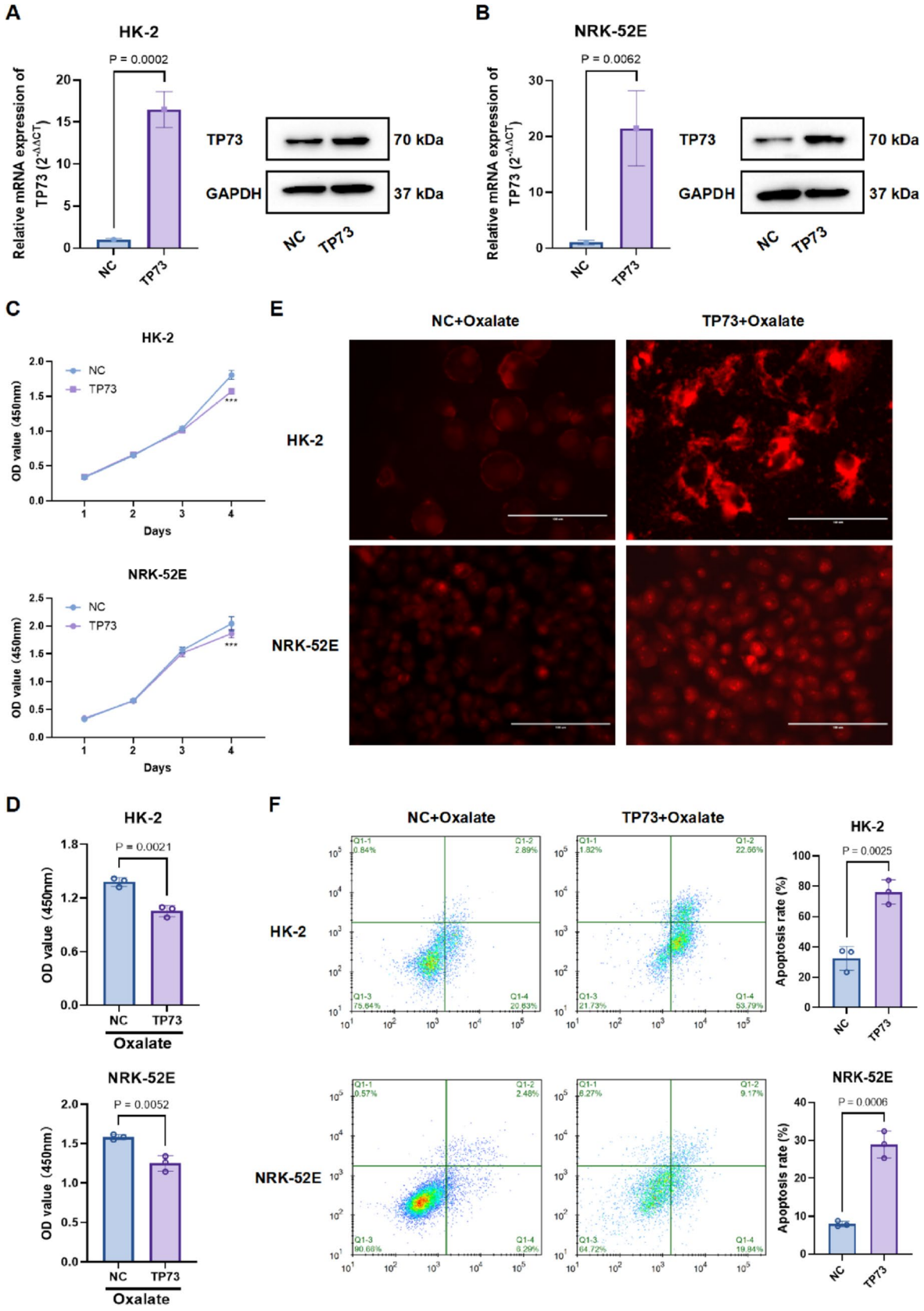
A
HK-2
P = 0.0002
Relative mRNA expression of TP73 ($2^{-\Delta\Delta CT}$)
NC
TP73
TP73
GAPDH
70 kDa
37 kDa
B
NRK-52E
P = 0.0062
C
HK-2
NRK-52E
OD value (450nm)
Days
NC
TP73
D
HK-2
NRK-52E
P = 0.0021
P = 0.0052
Oxalate
E
NC+Oxalate
TP73+Oxalate
F
Apoptosis rate (%)
P = 0.0025
P = 0.0006

◂**Fig. 7** Function of TP73 in oxalate-induced HK-2 and NRK-52E cells. **A**–**B** RT-qPCR and western blot assays validating TP73 expression in HK-2 (**A**) and NRK-52E (**B**) cells after different lentiviral transfection. **C**–**D** CCK-8 assays revealing TP73 significantly inhibited the proliferation of HK-2 cells and NRK-52E cells without oxalate (**C**) or with oxalate treatment (**D**). **E** DHE staining assessing the effect of TP73 on ROS generation in oxalate-induced cells (magnification × 400; scale bar, 100 μm). **F** Apoptotic rate of HK-2 and NRK-52E cells was determined by flow cytometry (mean ± SD, $n = 3$)

using both animal and cell models. Initially, we accessed the only two existing datasets of CaOx nephrolithiasis patients from GEO databases. Subsequently, employing WGCNA and four machine-learning algorithms, six hub DEGs were identified, including DLK2, BHLHA15, C12orf5, ICMT, LOXHD1, and TP73. Then, TP73 was identified as a significant hub gene in CaOx nephrolithiasis through ROC analysis (AUC = 0.885). Importantly, the expression and function of TP73 were validated in CaOx nephrolithiasis clinical samples, rat models, and cell models. Our study highlights TP73's role in promoting CaOx nephrolithiasis, providing insights into its pathogenesis and potential as a novel diagnostic biomarker.

In this study, efforts were made to identify diagnostic markers for CaOx nephrolithiasis. Based on the DEGs from GEO datasets, we utilized WGCNA and four machine-learning algorithms. The RF model, a non-parametric technique used for classification in a supervised manner, included decision trees constructed from segmented datasets [23]. We developed and analyzed a RF classification model to identify descriptors that distinguish CaOx nephrolithiasis samples from normal samples. Lasso logistic regression identified variables by minimizing classification error [24], and 11 overlapping DEGs were identified by Lasso regression. SVM-RFE was also utilized for feature ranking and selection, pinpointing the most significant features for classification [25], and 26 DEGs were obtained as potential diagnostic biomarkers in CaOx nephrolithiasis by SVM-RFE algorithm. Boruta is a feature selection algorithm, which iteratively removes features that are deemed less important than a random probe [26], and Boruta method displayed 11 DEGs that were associated with CaOx nephrolithiasis. Ultimately, DLK2, BHLHA15, C12orf5, ICMT, LOXHD1, and TP73 were selected as diagnostic markers in CaOx nephrolithiasis, and in-depth verifications confirmed their accuracy with ROC curves, nomogram, calibration and DCA curves. Several studies have investigated CaOx kidney stone biomarkers within GEO datasets, primarily utilizing GSE73680, but not GSE117518 [27–32]. Also, previous research predominantly employed WGCNA analysis without incorporating machine learning techniques or experimental validation [33]. In contrast, our study enhances gene identification related to renal calcification by integrating WGCNA with four machine learning algorithms and confirming findings across rat nephrocalcinosis models, cell lines, and human kidney samples. This multi-faceted approach ensures robust validation and consistent observations of TP73's role, thereby reinforcing the credibility of our results.

Previous studies have reported that CaOx nephrolithiasis development was closely associated with the apoptosis of renal tubular epithelial cells because cell apoptosis exposed matrix components that act as nucleation sites for calcium oxalate crystals, releases cellular debris that facilitates crystal aggregation, and alters the local chemical environment, thereby promoting crystallization [34–36]. Additionally, apoptosis-induced inflammation can exacerbate renal tubular injury, further increasing the propensity for stone formation [37]. The ability of TP73 to induce apoptosis was primarily attributed to its transactivation of pro-apoptotic genes [38, 39]. TP73 achieves this by transactivating genes within the nucleus, thereby enabling their action in the mitochondria or cytoplasm, ultimately leading to apoptosis [39]. It was reported that TP73 could induce osteosarcoma cell apoptosis and cell cycle arrest by either binding to TP53 response genes or transactivating them [40]. Researchers have also reported that the activation of TP73 could lead to cell apoptosis and suppresses tumor cell growth, clonogenic formation, and migration in prostate cancer cell lines [41]. Moreover, TP73 could act as a credible biomarker for predicting prognosis in cervical cancer [42] and glioma [43]. In this study, ROC curves revealed that TP73 exhibited the highest AUC values (0.885), suggesting its potential diagnostic utility. Also, our in vitro and in vivo experiments indicated an increased expression of TP73 in CaOx nephrolithiasis. Furthermore, we observed that TP73 significantly enhanced the apoptosis of oxalate-induced renal epithelial cells, suggesting a cytotoxic effect of TP73 in CaOx nephrolithiasis. Hence, we speculate that TP73 may promote CaOx kidney stone formation through apoptosis-related pathways, which needs further investigation.

Furthermore, studies have underscored the increasingly prominent role of immune cell infiltration in CaOx nephrolithiasis [44]. Nevertheless, to date, there has been limited application of CIBERSORT in investigating immune cell infiltration in CaOx nephrolithiasis and identifying potential diagnostic markers for this condition. In our study, GO and KEGG analysis showed that the DEGs between Normal group and the CaOx group samples were mainly involved in immune response. Then, infiltration of 22 familiar immune cell subtypes in the Normal group and the CaOx group samples was calculated by the CIBERSORT algorithm. Interestingly, we found that all six hub genes including TP73 were correlated with Th17 cells. The Th17 subset is significantly involved in inflammatory processes and contributes to immune-mediated renal tissue damage, ultimately leading

to various kidney diseases [45]. Previous studies have suggested that renal injury may facilitate the formation of kidney stones, particularly through alterations in urine composition and renal tubular dysfunction [46]. Additionally, tubular injury can impair the reabsorption process, leading to crystal nucleation and aggregation in the renal parenchyma [47]. Therefore, we hypothesize that renal injury from the interaction of TP73 and Th17 cells plays a significant role in the formation of CaOx nephrolithiasis, warranting further investigation.

In summary, we identified TP73 as a diagnostic biomarker in CaOx nephrolithiasis by integrating WGCNA and new scientific machine learning methodologies through combining the only two existing two datasets of CaOx nephrolithiasis patients. Previous studies focused on the effects of TP73 in human cancers; however, this study deepens our understanding of TP73 in the development of CaOx nephrolithiasis through bioinformatics analysis, and in vivo and in vitro investigations. What's more, we researched the role of TP73 in CaOx nephrolithiasis jointly from the three aspects of humans, animals and cells, providing a persuasive validation. However, the study lacks a comprehensive exploration of its underlying mechanisms, and further investigation aims at identifying TP73 target genes and mechanisms in CaOx nephrolithiasis. Additionally, the clinical relevance of TP73 is inadequately articulated, and we elucidate TP73 across rat nephrocalcinosis models, cell lines, and human samples, while the accumulation of disparate data could potentially obscure the underlying mechanisms of lithogenesis. In the future, we are expanding our collection of RPs from CaOx stone patients to perform RNA-Seq and proteomics to align experimental models with clinical observations, thereby improving the validity of TP73 as a potential biomarker in human CaOx nephrolithiasis.

Conclusion

In summary, we identified TP73 as a biomarker for CaOx nephrolithiasis. Comprehending the roles of TP73 in nephrolithiasis is crucial for a deeper understanding of the pathogenesis of CaOx nephrolithiasis and offers valuable insights for the development of related therapeutic strategies.

Supplementary Information The online version contains supplementary material available at https://doi.org/10.1007/s00240-024-01655-3.

Acknowledgements We thank Powerful Biology for help of IHC and dual immunofluorescence staining.

Author contributions ZZJ and WZ generated the idea, and designed the study. WLJ and CLK conducted the experiments and analysis. WLJ double checked the analysis. GP interpreted the results with the help of LHC. ZZJ drafted the paper, WZ and LHC critically revised the paper. All authors reviewed and approved the final version.

Funding This project was supported by grants from the National Natural Science Foundation of China (No. 82100807).

Data availability Data is provided within the manuscript or supplementary information files.

Declarations

Conflict of interests The authors declare no competing interests.

Ethical approval This study was approved by the Fudan Laboratory Animal Ethics Board and the Huashan Institutional Review Board of Fudan University (HIRB).

Consent for publication Not applicable.

References

1. Peerapen P, Thongboonkerd V (2023) Kidney stone prevention. Adv Nutr 14:555–569
2. Michibata U, Maruyama M, Tanaka Y, Yoshimura M, Yoshikawa H, Takano K, Furukawa Y, Momma K, Tajiri R, Taguchi K et al (2024) Calcium phosphate controls nucleation and growth of calcium oxalate crystal phases in kidney stones. Biomed Res 45:103–113
3. Sayer JA (2017) Progress in understanding the genetics of calcium-containing nephrolithiasis. J Am Soc Nephrol 28:748–759
4. Witting C, Langman CB, Assimos D, Baum MA, Kausz A, Milliner D, Tasian G, Worcester E, Allain M, West M et al (2021) Pathophysiology and treatment of enteric hyperoxaluria. Clin J Am Soc Nephrol 16:487–495
5. Wu M, Chen W, Zhang S, Huang S, Zhang A, Zhang Y, Jia Z (2019) Rotenone protects against β-cell apoptosis and attenuates type 1 diabetes mellitus. Apoptosis 24:879–891
6. Ming S, Tian J, Ma K, Pei C, Li L, Wang Z, Fang Z, Liu M, Dong H, Li W et al (2022) Oxalate-induced apoptosis through ERS-ROS-NF-κB signalling pathway in renal tubular epithelial cell. Mol Med 28:88
7. Song Q, Song C, Chen X, Xiong Y, Li L, Liao W, Xue L, Yang S (2023) FKBP5 deficiency attenuates calcium oxalate kidney stone formation by suppressing cell-crystal adhesion, apoptosis and macrophage M1 polarization via inhibition of NF-κB signaling. Cell Mol Life Sci 80:301
8. Bi Q, Wu JY, Qiu XM, Li YQ, Yan YY, Sun ZJ, Wang W (2023) Identification of potential necroinflammation-associated necroptosis-related biomarkers for delayed graft function and renal allograft failure: a machine learning-based exploration in the framework of predictive, preventive, and personalized medicine. Epma j 14:307–328
9. Tan Z, Chen X, Zuo J, Fu S, Wang H, Wang J (2023) Comprehensive analysis of scRNA-Seq and bulk RNA-Seq reveals dynamic changes in the tumor immune microenvironment of bladder cancer and establishes a prognostic model. J Transl Med 21:223
10. Guo H, Wang M, Shang Y, Zhang B, Zhang S, Liu X, Cao P, Fan Y, Tan K (2024) Apoptosis-related prognostic biomarkers and

potential targets for acute kidney injury based on machine learning algorithm and in vivo experiments. Apoptosis 29:303–320
11. Mao Y, Hou X, Fu S, Luan J (2024) Transcriptomic and machine learning analyses identify hub genes of metabolism and host immune response that are associated with the progression of breast capsular contracture. Genes Dis 11:101087
12. Zhao Y, Wei Y, Fan L, Nie Y, Li J, Zeng R, Li J, Zhan X, Lei L, Kang Z et al (2023) Leveraging a disulfidptosis-related signature to predict the prognosis and immunotherapy effectiveness of cutaneous melanoma based on machine learning. Mol Med 29:145
13. Abraham A, Kavoussi NL, Sui W, Bejan C, Capra JA, Hsi R (2022) Machine learning prediction of kidney stone composition using electronic health record-derived features. J Endourol 36:243–250
14. Elton DC, Turkbey EB, Pickhardt PJ, Summers RM (2022) A deep learning system for automated kidney stone detection and volumetric segmentation on noncontrast CT scans. Med Phys 49:2545–2554
15. Sassanarakkit S, Hadpech S, Thongboonkerd V (2023) Theranostic roles of machine learning in clinical management of kidney stone disease. Comput Struct Biotechnol J 21:260–266
16. Taguchi K, Hamamoto S, Okada A, Unno R, Kamisawa H, Naiki T, Ando R, Mizuno K, Kawai N, Tozawa K et al (2017) Genome-wide gene expression profiling of Randall's plaques in calcium oxalate stone formers. J Am Soc Nephrol 28:333–347
17. Leek JT, Johnson WE, Parker HS, Jaffe AE, Storey JD (2012) The sva package for removing batch effects and other unwanted variation in high-throughput experiments. Bioinformatics (Oxford, England) 28:882–883
18. Li Y, Yu J, Li R, Zhou H, Chang X (2024) New insights into the role of mitochondrial metabolic dysregulation and immune infiltration in septic cardiomyopathy by integrated bioinformatics analysis and experimental validation. Cell Mol Biol Lett 29:21
19. Zhang C, Xu T, Ji K, Cao S, Ai J, Pan J, Cao Y, Yang Y, Jing L, Sun JH (2024) Development and experimental validation of a machine learning-based disulfidptosis-related ferroptosis score for hepatocellular carcinoma. Apoptosis 29:103–120
20. Zhang WY, Chen ZH, An XX, Li H, Zhang HL, Wu SJ, Guo YQ, Zhang K, Zeng CL, Fang XM (2023) Analysis and validation of diagnostic biomarkers and immune cell infiltration characteristics in pediatric sepsis by integrating bioinformatics and machine learning. World J Pediatr 19:1094–1103
21. Zhou Z, Zhou X, Zhang Y, Yang Y, Wang L, Wu Z (2023) Butyric acid inhibits oxidative stress and inflammation injury in calcium oxalate nephrolithiasis by targeting CYP2C9. Food Chem Toxicol 178:113925
22. Anderegg MA, Olinger EG, Bargagli M, Geraghty R, Taylor L, Nater A, Bruggmann R, Sayer JA, Vogt B, Schaller A et al (2024) Prevalence and characteristics of genetic disease in adult kidney stone formers. Nephrol Dial Transplant
23. Tai AMY, Albuquerque A, Carmona NE, Subramanieapillai M, Cha DS, Sheko M, Lee Y, Mansur R, McIntyre RS (2019) Machine learning and big data: Implications for disease modeling and therapeutic discovery in psychiatry. Artif Intell Med 99:101704
24. Bose G, Healy BC, Lokhande HA, Sotiropoulos MG, Polgar-Turcsanyi M, Anderson M, Glanz BI, Guttman CRG, Bakshi R, Weiner HL et al (2022) Early predictors of clinical and MRI outcomes using least absolute shrinkage and selection operator (LASSO) in multiple sclerosis. Ann Neurol 92:87–96
25. Hosseini MP, Hosseini A, Ahi K (2021) A review on machine learning for EEG signal processing in bioengineering. IEEE Rev Biomed Eng 14:204–218
26. Huang RH, Hong YK, Du H, Ke WQ, Lin BB, Li YL (2023) A machine learning framework develops a DNA replication stress model for predicting clinical outcomes and therapeutic vulnerability in primary prostate cancer. J Transl Med 21:20
27. Hong SY, Xia QD, Xu JZ, Liu CQ, Sun JX, Xun Y, Wang SG (2022) Identification of the pivotal role of SPP1 in kidney stone disease based on multiple bioinformatics analysis. BMC Med Genomics 15:7
28. Hou C, Zhong B, Gu S, Wang Y, Ji L (2024) Identification and validation of the biomarkers related to ferroptosis in calcium oxalate nephrolithiasis. Aging (Albany NY) 16:5987–6007
29. Hong SY, Jiang HC, Xu WC, Zeng HS, Wang SG, Qin BL (2023) Bioinformatics analysis reveals the potential role of matrix metalloproteinases in immunity and urolithiasis. Front Immunol 14:1158379
30. Chen X, Li S, Shi C, Zhang W, Liu Z, Jiang J, Zhang Y, Chen Z, Zheng B, Zhu H (2023) Risk factors and predictors of urogenous sepsis after percutaneous nephrolithotomy for idiopathic calcium oxalate nephrolithiasis. Transl Androl Urol 12:1002–1015
31. Zhang Q, Wei H, Huang G, Jin L (2023) CCL7 and olfactory transduction pathway activation play an important role in the formation of CaOx and CaP kidney stones. Front Genet 14:1267545
32. Yang Y, Hong S, Lu Y, Wang Q, Wang S, Xun Y (2022) CAV1 alleviated CaOx stones formation via suppressing autophagy-dependent ferroptosis. PeerJ 10:e14033
33. Yu L, Li G, Jin S, Su J, Li S (2023) Identification of the core genes in Randall's plaque of kidney stone and immune infiltration with WGCNA network. Front Genet 14:1048919
34. Xie Z, Chen J, Chen Z (2022) MicroRNA-204 attenuates oxidative stress damage of renal tubular epithelial cells in calcium oxalate kidney-stone formation via MUC4-mediated ERK signaling pathway. Urolithiasis 50:1–10
35. Cao W, Zhang J, Yu S, Gan X, An R (2024) N-acetylcysteine regulates oxalate induced injury of renal tubular epithelial cells through CDKN2B/TGF-β/SMAD axis. Urolithiasis 52:46
36. Gao X, Lin B, Chen C, Fang Z, Yang J, Wu S, Chen Q, Zheng K, Yu Z, Li Y et al (2024) Lycopene from tomatoes and tomato products exerts renoprotective effects by ameliorating oxidative stress, apoptosis, pyroptosis, fibrosis, and inflammatory injury in calcium oxalate nephrolithiasis: the underlying mechanisms. Food Funct 15:4021–4036
37. Khan SR, Canales BK, Dominguez-Gutierrez PR (2021) Randall's plaque and calcium oxalate stone formation: role for immunity and inflammation. Nat Rev Nephrol 17:417–433
38. Rozenberg JM, Zvereva S, Dalina A, Blatov I, Zubarev I, Luppov D, Bessmertnyi A, Romanishin A, Alsoulaiman L, Kumeiko V et al (2021) The p53 family member p73 in the regulation of cell stress response. Biol Direct 16:23
39. Wood H (2021) TP73 variants implicate apoptosis in amyotrophic lateral sclerosis pathogenesis. Nat Rev Neurol 17:462
40. Shu Y, Ye W, Gu YL, Sun P (2018) Blockade of miR-663b inhibits cell proliferation and induces apoptosis in osteosarcoma via regulating TP73 expression. Bratisl Lek Listy 119:41–46
41. Wang Y, Radhakrishnan D, He X, Peehl DM, Eng C (2013) Transcription factor KLLN inhibits tumor growth by AR suppression, induces apoptosis by TP53/TP73 stimulation in prostate carcinomas, and correlates with cellular differentiation. J Clin Endocrinol Metab 98:E586-594
42. Ye H, Guo X (2019) TP73 is a credible biomarker for predicting clinical progression and prognosis in cervical cancer patients. Biosci Rep 39
43. Chen Y, Wang Y, He Q, Wang W, Zhang T, Wang Z, Dong J, Lan Q, Zhao J (2021) Integrative analysis of TP73 profile prognostic significance in WHO grade II/III glioma. Cancer Med 10:4644–4657
44. Sun Y, Liu Y, Guan X, Kang J, Wang X, Liu Q, Li D, Xu H, Tao Z, Deng Y (2020) Atorvastatin inhibits renal inflammatory response induced by calcium oxalate crystals via inhibiting the

activation of TLR4/NF-κB and NLRP3 inflammasome. IUBMB Life 72:1065–1074
45. Yang Y, Liu K, Chen Y, Gong Y, Liang Y (2019) Indoleamine 2,3-Dioxygenase (IDO) Regulates Th17/Treg Immunity in Experimental IgA Nephropathy. Folia Biol (Praha) 65:101–108
46. Kumar P, Patel M, Thomas V, Knight J, Holmes RP, Mitchell T (2020) Dietary oxalate induces urinary nanocrystals in humans. Kidney Int Rep 5:1040–1051
47. Mittal A, Tandon S, Singla SK, Tandon C (2016) In vitro inhibition of calcium oxalate crystallization and crystal adherence to renal tubular epithelial cells by Terminalia arjuna. Urolithiasis 44:117–125